Antifouling and Enhancing Pool Boiling by TiO_2 Coating Surface in Nanometer Scale Thickness

Wang Yan and Wang Lin-lin
School of Chemical Engineering and Technology, Tianjin University, Tianjin 300072, China

Liu Ming-yan
School of Chemical Engineering and Technology, Tianjin University, Tianjin 300072, China, and
State Key Laboratory of Chemical Engineering, Tianjin 300072, China

DOI 10.1002/aic.11345
Published online October 25, 2007 in Wiley InterScience (www.interscience.wiley.com).

The accumulation of unwanted crystallization deposits on heat transfer surface considerably reduces the efficiency of heat transfer in heat exchangers, especially in the evaporators with vapor–liquid boiling flows. To mitigate the fouling, some measures have been taken including utilizing low-energy surfaces made by a few kinds of surface-coating techniques. In this article, novel applications of TiO_2 material in inhibiting deposits on heat transfer surface as well as in enhancing pool boiling were developed with nanometer surface engineering method. TiO_2 coatings with different layer thicknesses in nanometer scale were prepared by applying vacuum coating technique and were characterized with respect to contact angle, surface free energy, roughness, film thickness, topography by contact angle analyzer, scanning electron microscopy (SEM), and atomic force microscopy (AFM), respectively. Distilled water pool boiling and $CaCO_3$ water solution fouling experiments in pool boiling system were performed on these coating surfaces and antifouling and heat transfer enhancement rules were investigated. The results indicate that all TiO_2 coating surfaces can avoid $CaCO_3$ deposition, and fouling induction period of TiO_2 coating surface in pool boiling with film thickness of 80×10^{-9} m is about 50 times longer than that of the untreated or polished surface in the present experimental conditions. On the other hand, pool boiling was enhanced on some TiO_2 coating surfaces with film thickness in nanometer scale, and heat transfer inhibiting was also observed with certain coating thickness. © 2007 American Institute of Chemical Engineers *AIChE J,* 53: 3062–3076, 2007
Keywords: nanometer, titanium oxide, vacuum coating, surface free energy, contact angle, SEM, AFM, fouling, pool boiling, enhancement

Introduction

Evaporators or evaporation concentrators are widely utilized in the process industry. However, fouling deposition on heat transfer surface and low process transfer efficiency are two unsolved problems in these heat exchangers. Fouling or scale is generally referred to the accumulation of undesirable deposits in solid phase or soft mud state on heat transfer surfaces in heat exchangers. The thermal conductivity of fouling layer formed on heat transfer surface is low, which can increase the resistance to heat transfer and will reduce the effectiveness of heat exchangers.[1–6] To inhibit or minimize scale deposition, a number of measures have been suggested, such as cleaning equipment with water or chemistry cleaning

Correspondence concerning this article should be addressed to Liu Ming-yan at myliu@tju.edu.cn.

agent, adding antifouling additive to the system, online cleaning with fluidized particles, avoiding fouling with electric, magnetic, and sound fields, developing nonfouling surface by using surface engineering technique, etc.[7] One of the desired approaches to reduce scale adhesion is to alter the property of the heat transfer surface to make it less attractive for the scale, so that fouling can be removed easily from the surface by boiling or flowing fluids. Since the surface free energy of a solid surface gives a direct measure of interfacial attractive forces, the adhesion force is largely dependent on the surface free energy of the heat transfer materials involved. Therefore, developing low free energy surface is one of the most potential antifouling methods and the research in this area is quite active in recent years. Most investigations on this area in pool or flow boiling systems demonstrate that the surface free energy has a significant influence on fouling adhesion on heat transfer surface and low-energy surfaces can significantly reduce the formation of fouling compared with the untreated or polished surfaces.[8–20]

Among these explorations, the most systematic and outstanding work was performed under the MODSTEEL project supported financially by European Community. In the project, various surface modification techniques including ion implantation, diamond-like carbon sputtering, plasma enhanced chemical vapor deposition, and autocatalysis were applied to reduce the fouling of process equipment in the dairy industry. The stainless steel surfaces were treated and characterized according to the chemical composition, roughness, topography, and wettability. For thick modified layers ($10{,}000 \times 10^{-9}$ m), only the elements of the coating were detected at the surface, whereas for thin layers ($100–2500 \times 10^{-9}$ m) the surface composition determined was that of the stainless steel substrate. The roughness of the 2R surfaces was $\sim 30–40 \times 10^{-9}$ m and not altered by the modification techniques (except for the Ni-P-PTFE coating, $53–100 \times 10^{-9}$ m). For the 2B surfaces an increase in roughness was observed (about $48–550 \times 10^{-9}$ m). DLC sputtering (about 450×10^{-9} m) and Ni-P-PTFE coating (about 230×10^{-9} m) produced surfaces with the highest roughness. All modified surfaces revealed a similar surface topography with the exception of the Ni-P-PTFE coating, for which the coating masked the underlying steel topography. Regarding the wettability, the SiOx-plasma CVD and Ni-P-PTFE coating techniques produced the most hydrophilic and hydrophobic surfaces, respectively.[16] These modified stainless steel-based surfaces were evaluated according to their fouling behavior for different dairy products under different conditions. Aqueous solutions that simulate milk were used to study the fouling behavior during pasteurization. The results showed that for the nonmicrobiological deposits the Ni-P-PTFE surface was the most promising one, since it generally promoted less deposit build-up and was the easiest to clean. On the other hand, for bacterial adhesion, the most suitable surface was the ion-implanted surface, which also showed less spores after the cleaning process.[20]

The surface techniques applied in these studies include ion implantation, magnetron sputtering, ion plating, electroplating, electroless plating, selfassembling, dipping, liquid phase deposition etc. And some potential coatings materials are fluorine, fluorinated diamond-like carbon, and Ni-P-PTFE etc.[9,10,14,15] However, there are still some key questions to be answered for the surface with additional coatings. For example, how does the antifouling effectiveness vary with the increase of the coating thickness? Under what coating thickness, can the additional thermal resistance to heat transfer with low conductivity layer be ignored? And under what coating thickness, can boiling heat transfer be enhanced on these antifouling surfaces? As for the surface without additional film layer, one of the concerned issues is how to keep the effectiveness and lastingness of the antifouling low energy surface.

On the other hand, much progress on boiling heat transfer enhancement has been made in the past about 50 years, and the enhancement methods include passive, active, and compound enhancement techniques.[3,21] Among the passive techniques, surface enhancement has been emphasized. Since the first high-performance heater surface configurations were patented in the late 1960s, a great variety of evaporator tubes with enhanced surfaces have been developed, that can be divided in two main groups, one based on integral-fin tubes with modified fins to form reentrant grooves or tunnels ("structured surfaces"), and the other based on plain tubes with sintered, plasma spraying or flame spraying porous metallic matrix bonded to the tube surface ("coated porous surfaces"). Such coatings possess heat transfer coefficients up to 10 times those for smooth untreated surfaces and there is an optimum coating thickness to achieve maximum heat transfer coefficient.[22–26] Pool boiling heat transfer from nano-porous surface immersed in a saturated FC-72 dielectric fluid has been experimentally studied at atmospheric pressure lately. The data obtained from nano-porous surface of thickness about 70×10^{-6} m made from aluminum oxide were compared with that of a plain aluminum surface of thickness about 105×10^{-6} m. It was found that there is a reduction of about 30% in the incipient superheat for the applied power for nano-porous surface over plain surface.[27]

Recently, TiO_2 coatings with superhydrophilicity by exposing the surface to UV ray were explored to enhance pool boiling by using dipping and magnetron sputtering, and it is found that the critical heat flux (CHF) of TiO_2-coated surface is about two times larger than that of noncoated one, and the temperature at minimum heat flux (MHF) for the superhydrophilic surface is higher by 100 K than that for the normal one and the superhydrophilic surface can be an ideal heat transfer surface.[28–30] The pool boiling on a superhydrophobic coating surface was also investigated. The surface was coated with fine particles of nickel and PTFE by means of electrolytic plating with contact angle to water of 152° in room temperature and thickness of 10×10^{-6} m. It seems from the primary results that the boiling feature on superhydrophobic surface is quite different from that of usual surfaces. The stable film boiling occurs in very small superheating, and there is no nucleate boiling region. The bubbles generated on the surface coalesce into a vapor film without departing from the surface. The stable vapor film exists even at a surface temperature below the saturation temperature.[31] It indicates that superhydrophilic surface is advantageous to boiling or evaporation but superhydrophobic surface is not.

It is noteworthy that antifouling function should also be considered on developing enhanced surfaces[21] because for most boiling evaporation processes, fouling on heat transfer

surface is easy to be formed. In this situation, hydrophobic surface or low energy surface may be favorable.

It is well known that the nanometer material has unique selfcleaning effect, which has been applied to the glass windows of buildings, car coatings, clothes, and so on. And recent studies show that the main reasons resulted in the self-cleaning functions of natural bio-surfaces such as lotus leaves, rice leaves, cicada wings, and water strider legs were contributed to their superhydrophobic natures and the micro- and nano-scale structures.[32] Hence, increasing the hydrophobicty of the heat transfer surface with nanometer material may improve the nonfouling characteristic. Meanwhile, the improved antifouling surfaces may enhance boiling heat transfer as well if the surface coating thickness is in nanometer order. In our very recent work, T_iO_2 coating surface with layer thickness in micrometer scale was prepared by liquid phase deposition (LPD) method and flow boiling enhancement and antifouling on such coating surfaces were investigated and confirmed.[33]

The main goal of this work is to explore the antifouling and pool boiling heat transfer enhancement characteristics on low energy surfaces of TiO_2 coating with layer thickness in nanometer scale. First, low energy surfaces of TiO_2 coatings with different layer thicknesses in nanometer order were prepared by applying vacuum coating technique. Second, they were characterized by using contact angle analyzer, SEM, and AFM. Finally, distilled water pool boiling and $CaCO_3$ water solution fouling experiments in pool boiling system were performed on these coating surfaces to investigate the antifouling and heat transfer enhancement effects.

Preparation and characterization of TiO_2 coating surfaces

Preparation of TiO_2 Coating Surfaces. Three types of tested surfaces were prepared: untreated, polished, and coated surfaces, and they are all red copper-based surfaces. For the polished surface, the modifications consist of finishing by using emery wheel with emery grits of Nos. 340 and 600, polishing by using polishing wheel with grinding pastes of emery sand particles in diameters of 1×10^{-6} m and 0.5×10^{-6} m, removing oil by using 10% NaOH water solution immersion and acetone ultrasonic cleaning, cleaning with deionized water, and airing with natural air. TiO_2 coatings were prepared on polished red copper-based surfaces using vacuum coating technique.

The vacuum coating on polished surface with TiO_2 material was carried out at Tianjin University, China, using a ZZS700-2/G type vacuum box coater made by Cheng-du Nan Guang Industry. The vacuum coating is a physical vapor deposition (PVD) process at a high vacuum. The ZZS700-2/G type vacuum box coater is composed of main machine box, control-electricity tank, and high-voltage control tank. The final vacuum is 9.5×10^{-5} Pa with liquid nitrogen, 5×10^{-4} Pa without liquid nitrogen. In the main machine box, there is an evaporation chamber with the diameter of 0.71 m and height of 0.85 m, a workpiece frame which can rotate in the maximum number of revolution per minute 30 driven by a direct current electric motor and a few jigs with diameter of 0.64 m for both spherical cap and flat workpieces, two E-type magnetic deflection electron beam evaporation sources with electron gun power of 6, 8, or 10 kW with a *X–Y* magnetic deflection scan unit, an electron gun filament and a beam flow control unit, a gas extracting system and a cooling system etc. The workpiece surface to be coated (the substrate) and the coating material (in the evaporation source) of high-purity (99.999%) TiO_2 are arranged in the vacuum evaporation chamber of the main machine box. During vacuum coating, the thermoelectrons emitted from the filament are accelerated when passing through the electric field and bombard the evaporation material surface after being deflected in their electronic orbits in certain angle affected by the electromagnetic field and focused. The evaporation material is heated to a rather high temperature by the focused, accelerated high-energy electron beam and evaporates in the high vacuum chamber. At last vaporized TiO_2 material deposits on the substrate with very thin film layer. The coating thickness is monitored by the quartz crystal thickness monitor and controlled by the coating time. The substrate is not heated during vacuum coating and its temperature is about ambient temperature.

Table 1. Vacuum Coating Parameter and TiO_2 Coating Thickness

Vacuum/ $\times 10^{-3}$ Pa	Coating time/s	Evaporating velocity/ $\times 10^{-10}$ m s^{-1}	Designed Coating thickness/ $\times 10^{-9}$ m	Real Coating thickness/ $\times 10^{-9}$ m
2.5	1653	0.6	100	99.9
2.6	1763	0.5	80	80.4
4.1	1553	0.3	60	60.5
2.2	800	0.5	40	39.9
2.8	166	1.2	20	20.7

In this work, TiO_2 coating surfaces with different layer thicknesses in nanometer scale were formed on the red copper substrates with diameter of 0.11 m and thickness of 0.006 m to study the effect of coatings in nanometer order thickness on antifouling and enhancing pool boiling heat transfer. Meanwhile, small rectangular coating samples based on the red copper plate with the length of 0.01 m, width of 0.01 m, and height of 0.006 m were simultaneously prepared for easy measurement and analysis. The vacuum coating parameter and coating thickness are shown in Table 1. It can be found that the real coating thickness is close to the designed and varies with the coating time. The thickness ranges from 20 to 100×10^{-9} m. The real coating thickness is the thickness displayed on the digital control board in the coating instrument. Typical AFM measurement value of coating thickness is near the same as that displayed on the instrument control board, which is illuminated in Figure 7.

Measurement of contact angle and calculation of free energy of TiO_2 coating surface

The contact angles of untreated, polished, and coated surfaces with different layer thicknesses of TiO_2 were measured by using JY-82 contact angle analyzer and the distilled water and glycerine were used as titers. The measurement of each contact angle was repeated three times and the averages of different coating surfaces are shown in Table 2. To have a qualitative grip of such coating surfaces, typical digital photos of coating surfaces and distilled water drops on these

Table 2. Contact Angle and Surface Free Energy of TiO_2 Coating Surfaces

$\delta/\times 10^{-9}$ m	$\theta_w/^\circ$	$\theta_g/^\circ$	$\gamma/\times 10^{-3}$ Jm^{-2}
Untreated	58.2	100.0	207.7
Polished	60.8	101.5	199.1
100	83.7	115.5	119.8
80	86.3	118.0	115.4
60	88.5	120.3	112.4
40	89.0	120.5	110.1
20	91.7	121.0	95.5

surfaces taken in natural light are illustrated in Figure 1. The color of TiO_2 coating surface gets darker with increase of the film thickness, as shown in Figure 1a. Table 2 shows that the contact angle of untreated surface is lowest and polishing treatment increases the contact angle of surface; coating process further enlarges the contact angle and thus improves the hydrophobicity; the contact angle of coating surface increases slightly with the decrease of the coating thickness and the contact angle of the thinnest coating surface with thickness of 20×10^{-9} m is the largest one.

The surface free energy was calculated on the measurement data of contact angles of coating surfaces according the Young's equation, Owense equation, GEO_m method, and GEO_s method[34] and also given in Table 2. It can be seen from Table 2 that compared with the untreated and polished surfaces, coating process reduces the surface free energy greatly due to the appearance of the TiO_2 material in the thickness of nanometer order on the red copper surface. However, the surface free energy reduction is not obvious with the decrease of the thickness of coating surface under the present range of film thickness. Figure 2 clearly illuminates this variation tendency, in which, -20×10^{-9} m and 0×10^{-9} m of abscissa values, not being the concrete values of coating thickness, only represent the untreated and polished heat transfer surfaces, respectively. The effect of coating thickness on surface energy seems unusual because surface energy describes the interaction of the fluid with the first coating of the substrate, but this trend was also found in the TiO_2 coating in micrometer scale made by LPD method.[33] One reason is that the surface free energy is determined by the properties of the TiO_2 nanometer scale material itself and these properties such as density and hardness change with the increase of the coating thickness. When the coating is thin, it may not be the film layer traditionally referred to. Meanwhile, the varying range of the coating thickness is not wide in this work and the surface energy variation with the increase of the layer thickness is very weak.

Characterizations of TiO_2 coating surfaces by SEM and AFM

SEM. To get the topography information of TiO_2 coating surface, SEM measurements were performed first. Figure 3 shows the SEM images of untreated, polished, and TiO_2 coating surfaces in micrometer scale with two different film thicknesses of 20×10^{-9} m and 80×10^{-9} m before the pool boiling and fouling experiments, respectively. The coated surfaces (Figures 3c, d), like polished one (Figure 3b), are very glazed, which is quite different from the untreated one (Figure 3a) that is scraggly. Figure 3 indicates that coating TiO_2 material on polished surface has no great effect on the surface morphology compared with the polished one, and all coated surfaces seem very uniform in film thickness. Other coated surfaces hold the same surface morphologies on the SEM images as the ones mentioned earlier and will not be shown again.

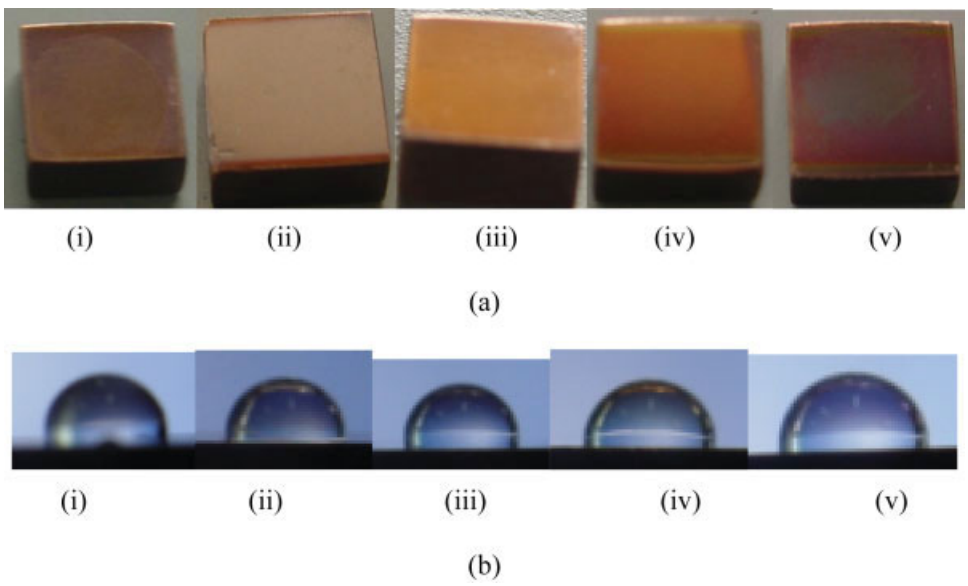

Figure 1. Digital photos of TiO_2 coating surfaces and distilled water drops on the surfaces.

(a) TiO_2 coating surfaces with different film thicknesses; (b) distilled water drops on TiO_2 coating surfaces with different film thicknesses. (i) 20×10^{-9} m; (ii) 40×10^{-9} m; (iii) 60×10^{-9} m; (iv) 80×10^{-9} m; (v) 100×10^{-9} m. [Color figure can be viewed in the online issue, which is available at www.interscience.wiley.com.]

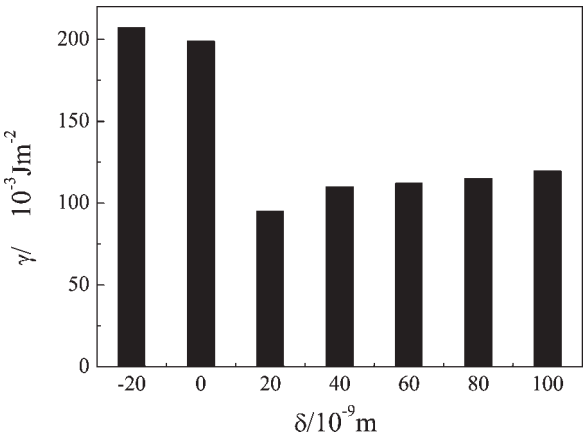

Figure 2. Relationship of TiO_2 coating thickness and the surface free energy.

AFM

To get more detailed information on microstructure of TiO_2 coating surface, AFM is utilized and TiO_2 coating surface with film thickness of 80×10^{-9} m is taken as an example to find the proper scan area for enough analysis. The scan area change from 100×100 $(10^{-9}$ m$)^2$ to 30,000 $\times$ 30,000 $(10^{-9}$ m$)^2$. Typical two- and three-dimensional AFM images of TiO_2 coating surfaces with coating thickness of 80×10^{-9} m under 2000×2000 $(10^{-9}$ m$)^2$ (Figures 4a, b), 10,000 $\times$ 10,000 $(10^{-9}$ m$)^2$ (Figures 4c, d), 20,000 $\times$ 20,000 $(10^{-9}$ m$)^2$ (Figures 4e, f) scan areas are shown in Figure 4. It can be found from Figure 4 that with the widening of the scan area, surface microcosmic pattern becomes clearer and richer. As shown in Figure 4a, TiO_2 coating surface consists of ellipsoid or hillock units distributed homogeneously, which is much like the case of the surface coated with fluorinated diamond-like carbon film at the scan area of 2000×2000 $(10^{-9}$ m$)^2$.[15] It seems that to get the microcosmic pattern, the scan area of $2000 \times 2000(10^{-9}$ m$)^2$ is enough. If further enlarging the scan area, much more information appears on the AFM images, such as valleys, cracks, and sharp peaks along the surfaces, as shown in Figures 4c, e. The largest ellipsoid in Figure 4e is the cluster of TiO_2 crystallites.

The data of the root mean square roughness (R_{rms}) being the standard deviation of the height values within a given scan area and difference in height between the highest and lowest points on the surface relative to the mean plane (R_{max}) given in the AFM images are utilized to quantify the surface roughness. R_{rms} of 80×10^{-9} m TiO_2 coating for the four scan areas (100×100 $(10^{-9}$m$)^2$, 2000×2000 $(10^{-9}$ m$)^2$, 10,000 $\times$ 10,000 $(10^{-9}$ m$)^2$, and 20,000 $\times$ 20,000 $(10^{-9}$ m$)^2$) are 1.0×10^{-9} m, 2.4×10^{-9} m, 4.7×10^{-9} m, and 5.7×10^{-9} m, respectively. These data indicate that with the rising of scan area, the surface roughness approaches to a steady value in nanometer scale. R_{max} of 80×10^{-9} m TiO_2 coating for the four scan areas are 6.1×10^{-9} m, 32.5×10^{-9} m, 118.0×10^{-9} m, and 135.7×10^{-9} m, respectively. R_{max} increases when enlarging the scan area. When the scan area exceeds

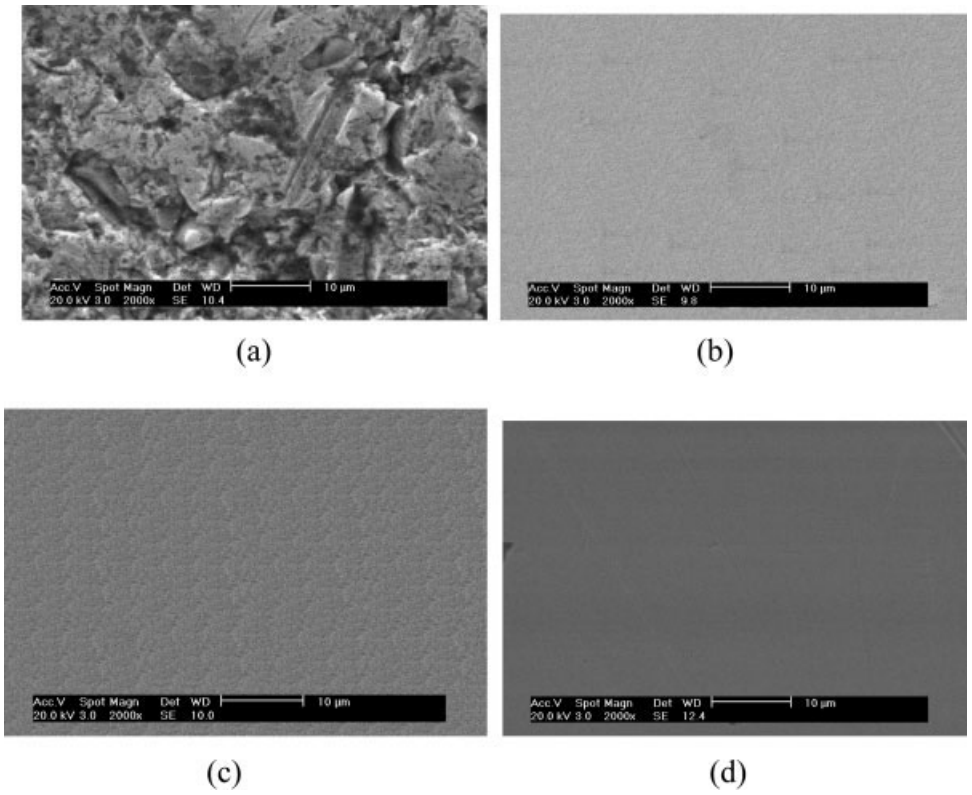

Figure 3. Typical SEM images of untreated, polished, and TiO_2 coating surfaces.

(a) untreated; (b) polished; (c) 20×10^{-9} m; (d) 80×10^{-9} m.

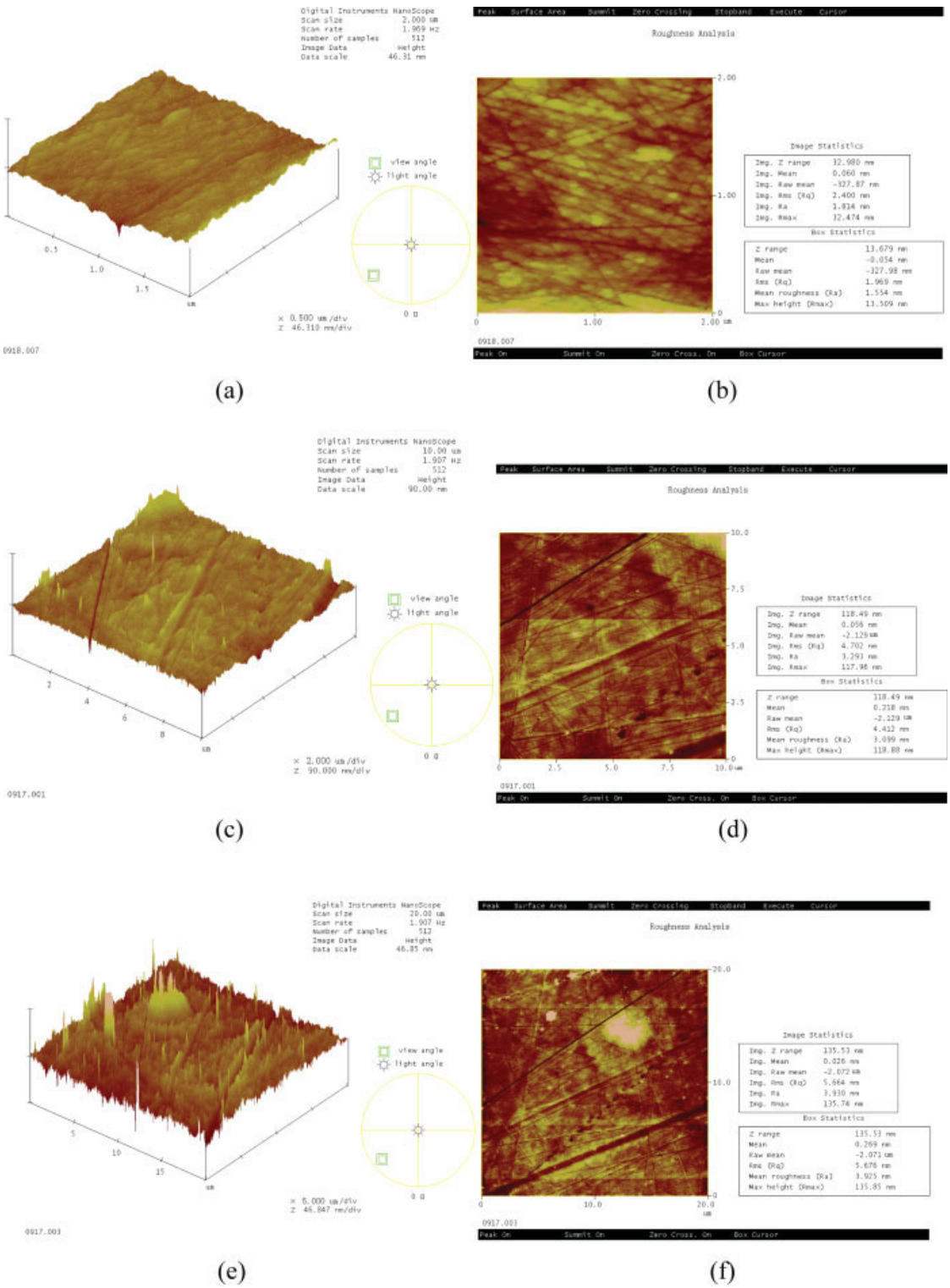

Figure 4. Two- and three-dimensional AFM images of TiO_2 coating surfaces with film thickness of 80 × 10^{-9} m under different scan areas.

(a), (c), and (e) are three-dimensional AFM images; (b), (d), and (f) are two-dimensional AFM images; (a) and (b) with scan area of 2000 × 2000 $(10^{-9}$ m$)^2$; (c) and (d) with scan area of 10,000 × 10,000 $(10^{-9}$ m$)^2$; (e) and (f) with scan area of 20,000 × 20,000 $(10^{-9}$ m$)^2$. [Color figure can be viewed in the online issue, which is available at www.interscience.wiley.com.]

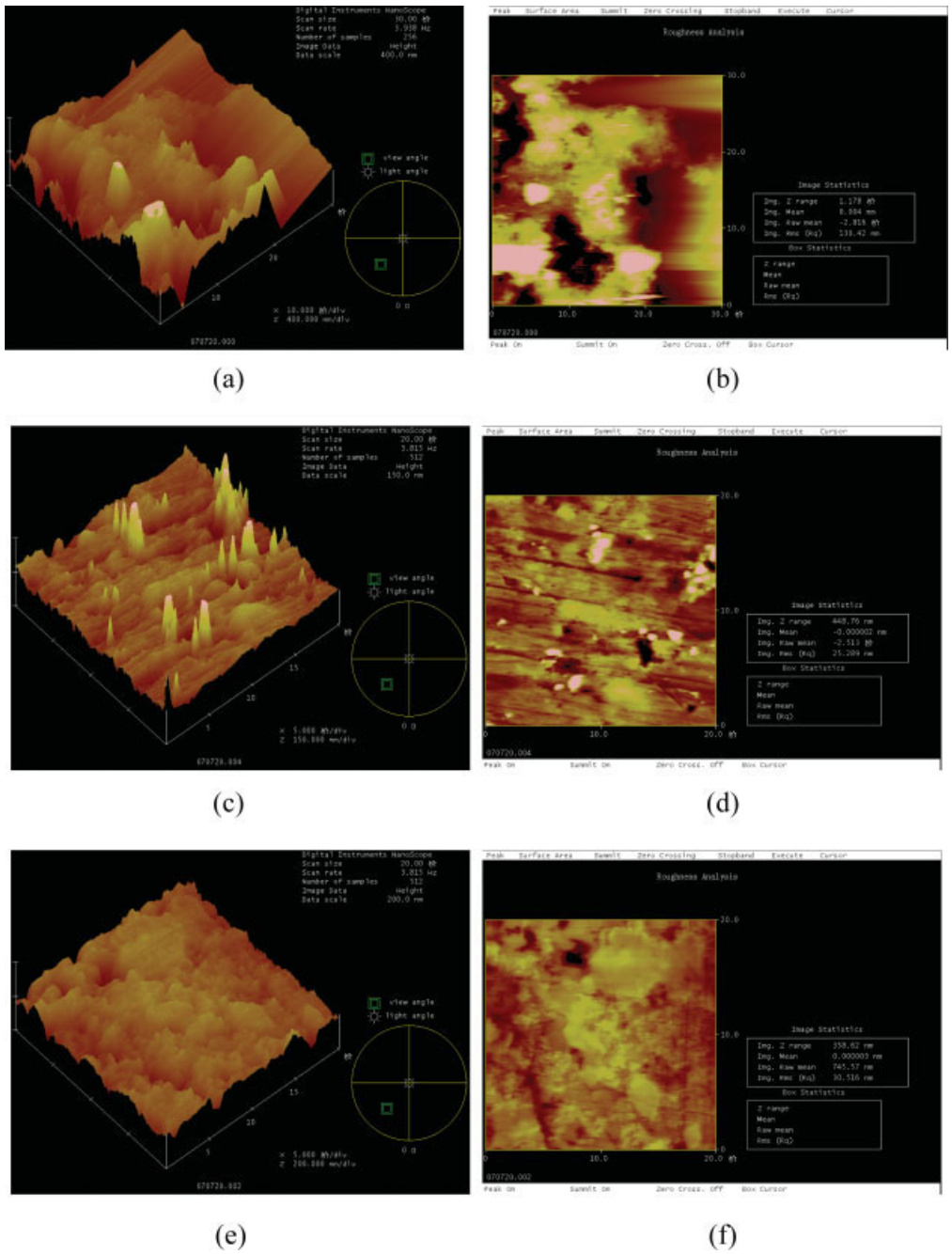

Figure 5. Two- and three-dimensional AFM images of all heat transfer surfaces.

(a) and (b) untreated surface; (c) and (d) polished surface; (e) and (f) TiO_2 coating surface with layer thickness of 20×10^{-9} m; (g) and (h) TiO_2 coating surface with layer thickness of 40×10^{-9} m; (i) and (j) TiO_2 coating surface with layer thickness of 60×10^{-9} m; (k) and (l) TiO_2 coating surface with layer thickness of 80×10^{-9} m; (m) and (n) TiO_2 coating surface with layer thickness of 100×10^{-9} m. [Color figure can be viewed in the online issue, which is available at www.interscience.wiley.com.]

$10{,}000 \times 10{,}000$ $(10^{-9}\ \text{m})^2$, both R_{rms} and R_{max} rise weakly, which indicates that the scan area of $10{,}000 \times 10{,}000$ $(10^{-9}\ \text{m})^2$ is enough to carried out proper analysis.

The data of surface roughness of all heat transfer surfaces used in this work were obtained by AFM analyses with scan area of $20{,}000 \times 20{,}000$ $(10^{-9}\ \text{m})^2$ or $30{,}000 \times 30{,}000$ $(10^{-9}\text{m})^2$. Two- and three-dimensional AFM images are shown in Figure 5. The relationship between R_{rms} or R_{max} and coating thickness is shown in Figure 6.

In Figure 6, -20×10^{-9} m and 0×10^{-9} m of abscissa values, not being the real values of coating thickness, only represent the untreated and polished heat transfer surfaces, respectively, and the connection lines of data points are just for directing the eyes.

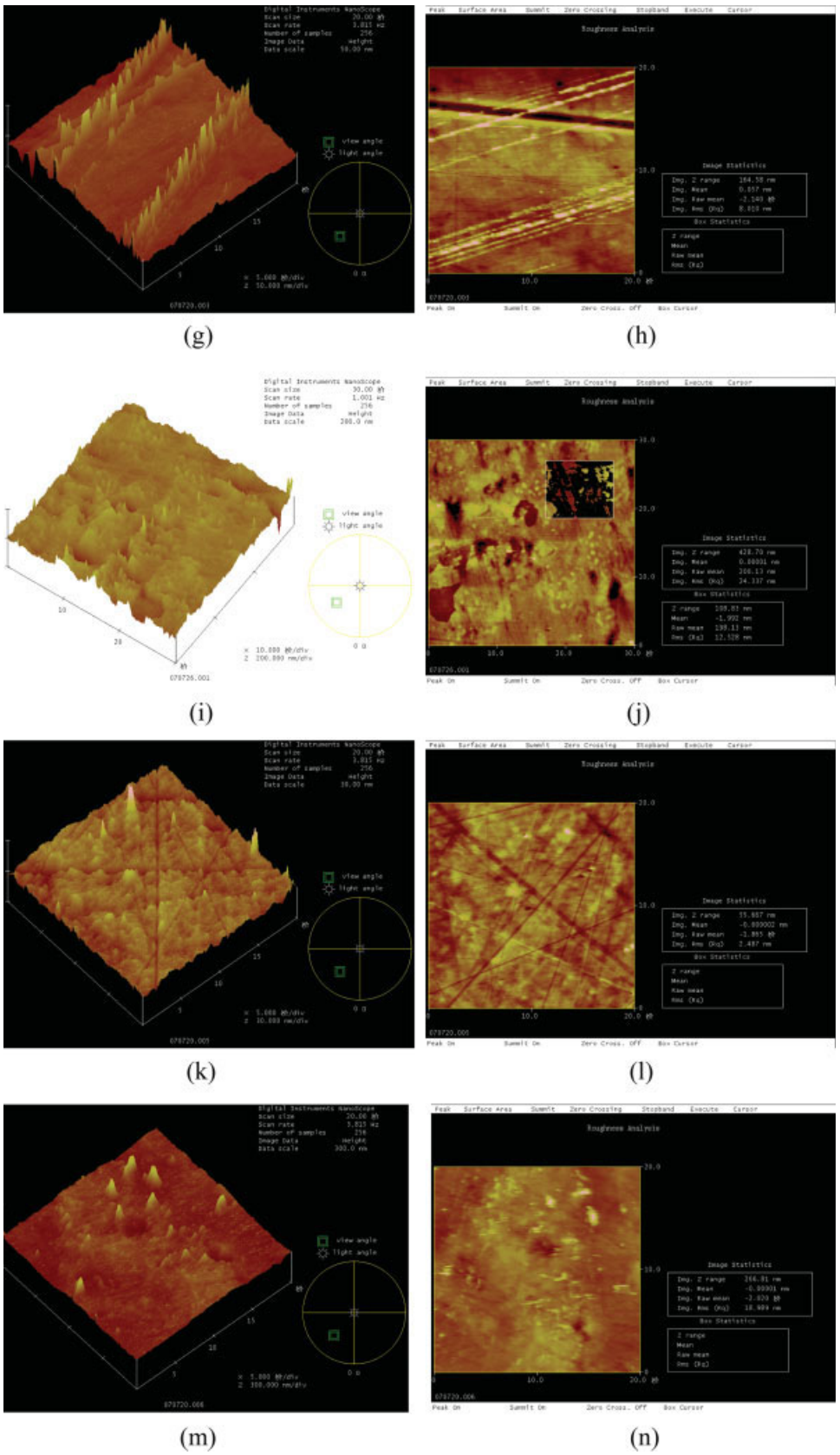

Figure 5. (Continued)

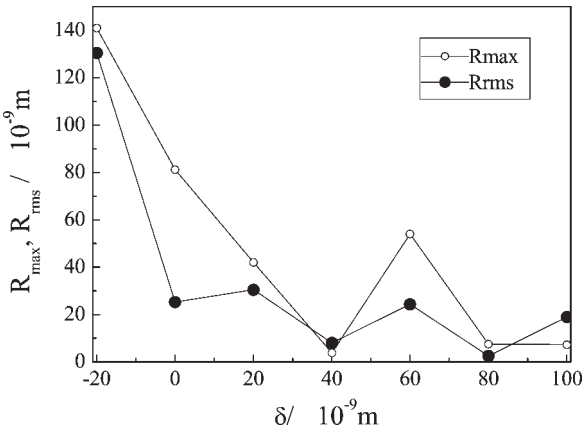

Figure 6. Relationship between surface roughness and coating thickness of all heat transfer surfaces.

It can be seen from Figures 5 and 6 that the topography of untreated surface (Figure 5a) is most different from the other heat transfer surfaces and the other heat transfer surfaces have the similar morphology, including the polished surface. The untreated sample (Figure 5a) exhibits a rugged surface topography in which some mountains and valleys are observed, while other samples reveal more homogeneous appearances full of hillock units along the surfaces. This is in accordance with the roughness values as shown in Figure 6, and untreated sample holds the highest R_{rms} and R_{max}, while other samples' roughness values are near and are in the nanometer scale. This indicates that vacuum coating process did not affect the red copper substrate topography significantly. From two-dimensional images shown in Figure 5, it can be found that with the increase of the coating thickness, the real color of the red copper substrate becomes dark. Of course, the TiO_2 coating with thickness of 100×10^{-9} m can't mask all surface features of the red copper support (Figure 5n).

Figure 6 shows that R_{rms} and R_{max} decrease generally, slightly and wavily with the rising of the coating thickness. Among the heat transfer surfaces, 80×10^{-9} m coating surface has the lowest R_{rms}, second, 40×10^{-9} m coating surface.

It is noteworthy that the AFM image measurements in Figure 5 were carried out after making the digital photos of distilled water drops on the heat transfer surfaces, which is different from the measurement condition of AFM images given in Figure 4. Hence, the AFM images and results of surface roughness were affected in certain degree by the leftover of water drop. For example, for the same coating surface with coating thickness of 80×10^{-9} m, there are more sharp needles when the rectangular coating sample was new (Figure 4e) than after it was used for contact angle analysis (Figure 5k) in the three-dimensional AFM image. One reason for this is that the remains of the water drop on the sample might smooth the surface, and the other is that the scan location is not the same. But the variation tendency of surface roughness may not largely be affected.

The TiO_2 coating thickness is also measured with AFM to test the control accuracy of the vacuum coating process by scanning the brim of the coated samples or the edge between the red copper substrate and the coatings. Figure 7 shows typical two- and three-dimensional AFM images. The measurement value of film thickness is 80.0×10^{-9} m, which is close the datum (80.4×10^{-9} m, as shown in Table 1) displayed on the control board during vacuum coating.

Apparatus and measuring system of pool boiling heat transfer and fouling experiments

The schematic diagram of pool boiling and fouling experimental apparatus and heat transfer block are shown in Figure 8.

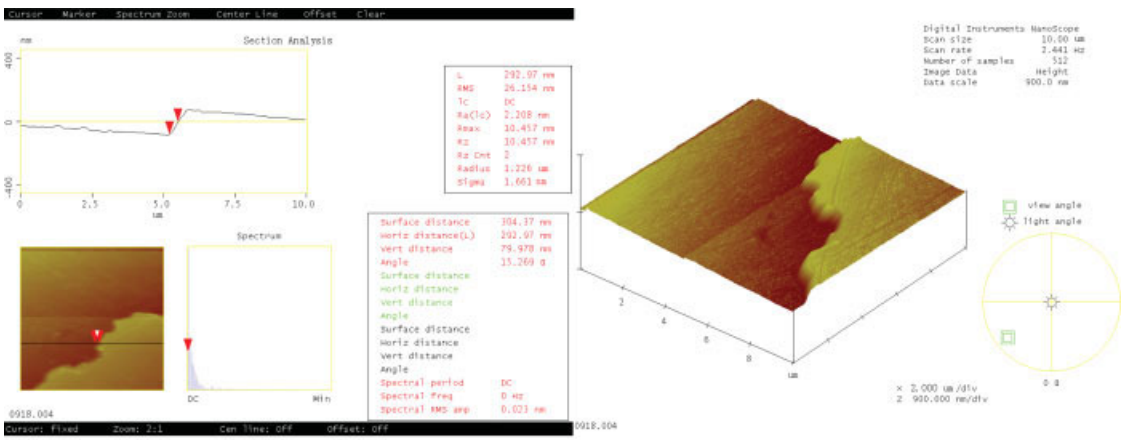

Figure 7. Two- and three-dimensional AFM images of TiO_2 coating surfaces with layer thickness of 80×10^{-9} m by scanning the edge.

(a) Two-dimensional; (b) three-dimensional. [Color figure can be viewed in the online issue, which is available at www.interscience.wiley.com.]

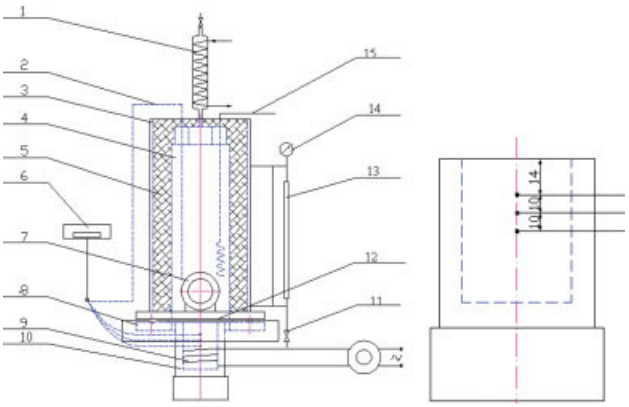

Figure 8. Experimental apparatus and heat transfer block.

1-Condenser; 2-Pt 100 type platinum resistance; 3-Coat of pool boiling apparatus; 4-Boiling pool; 5-Thermal insulation material; 6-Industrial computer 610 system; 7-View window; 8-Flange; 9-Resistance wire; 10-Heat transfer block; 11-Valve; 12-Copper plate; 13-Level-meter; 14-Manometers; 15-Preheater. (a) Experimental apparatus (b) Heat transfer block (unit, mm). [Color figure can be viewed in the online issue, which is available at www.interscience.wiley.com.]

The experimental apparatus mainly consists of a cylindrical stainless steel tank with inner diameter of 0.1 m and height of 0.3 m, a resistance wire heater with maximum heating power of 600 W, a heat transfer red copper block with diameter of 0.08 m and a height of 0.06 m, a heat transfer copper plate with diameter of 0.11 m and thickness of 0.006 m and a condenser with heat transfer area of 0.02 m^2.

The temperature measuring system consists of a few Pt resistance transducers, a signal amplifier, an A/D converter and an industrial computer 610. The heat transfer surface of copper block is mirror smooth, facing upward. The temperatures along the center axis of the heat transfer block were measured by three Pt resistances embedded in the copper block, as shown in Figure 8b. The temperature of the liquid in boiling pool was also measured by Pt resistance. The measurement was conducted in a steady state, which was judged by monitoring the output of Pt resistance. The temperature data were recorded with a sample frequency of 10 Hz and length of 100 points for each 1800 s.

Pool boiling and fouling experiments on different heat transfer surfaces were carried out and boiling phenomena were observed through view windows. Distilled water was used for pool boiling investigations and calcium carbonate solution was used for fouling experiments in pool boiling. $CaCO_3$ test solution was prepared by dissolving a certain amount of analytical grade $CaCl_2$ and $NaHCO_3$ in distilled water with temperature of 293 K. The concentrations for $CaCl_2$ and $NaHCO_3$ were 72.2 and 54.6 $\times$ 10^{-3} kg/m^3, respectively. The concentration of the saturated $CaCO_3$ water solution of was 65 $\times$ 10^{-3} kg/m^3.

Heat flux through heat transfer surface and surface temperature were determined by using three temperatures in the heat transfer black and their axial locations according to one-dimensional conduction theory. Heat flux was calculated by the equation

$$q_i = \lambda \frac{T_{i+1} - T_i}{\chi_{i+1} - \chi_i} \tag{1}$$

And average heat flux was

$$q = \frac{\lambda}{n-1} \sum_{i=1}^{n-1} \left(\frac{T_{i+1} - T_i}{\chi_{i+1} - \chi_i} \right) \tag{2}$$

The temperature of pool boiling surface was

$$T_w = \frac{1}{n-1} \sum_{i=1}^{n-1} \left[T_i - \frac{\chi_i}{\chi_{i+1} - \chi_i} (T_{i+1} - T_i) \right] \tag{3}$$

Thus, average heat transfer coefficient of pool boiling was

$$h = q/\Delta T_w \tag{4}$$

where

$$\Delta T_w = T_w - T_s \tag{5}$$

Resistance of TiO_2 film thickness is estimated by

$$R_f = \frac{1}{h} - \frac{1}{h_0} \tag{6}$$

Heat flux varied from 0 to 110 kW m^{-2} in this work.

Results and Discussion

To testify the reliability of the experimental apparatus and to find the pool boiling state of the present work, pool boiling of distilled water on untreated copper-based surface was first investigated. The experimental data were compared with those reported in literature,[35] as shown in Figure 9. Figure 9 indicates that the datum agreement is good and the transition point between natural convection and nucleate boiling can basically be determined. The heat transfer experiments in this work were carried out in the nucleate boiling regime.

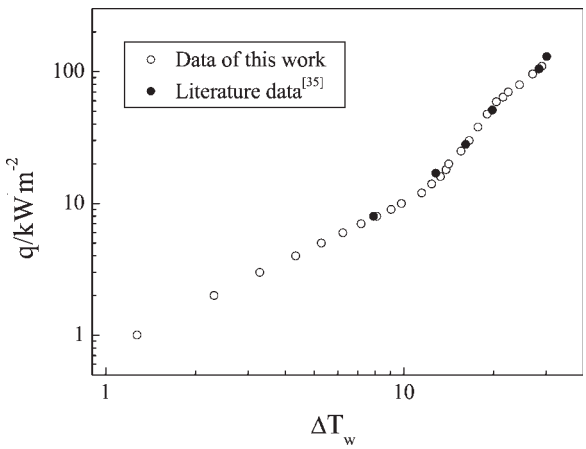

Figure 9. Pool boiling data on untreated copper based surface.

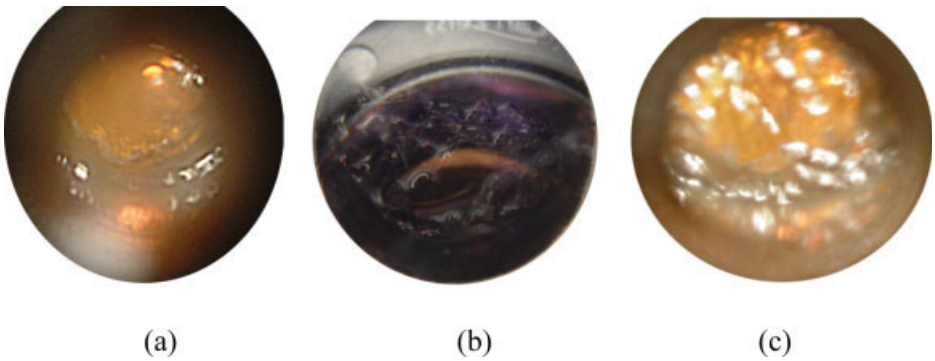

Figure 10. Typical pool boiling images (top view) on polished copper surfaces when varying the heat flux.

(a) q = 79.8 kW m^{-2}; (b) q = 96.6 kW m^{-2}; (c) q = 110 kW m^{-2}. [Color figure can be viewed in the online issue, which is available at www.interscience.wiley.com.]

Typical pool boiling images (top view) on polished copper when varying heat flux are shown in Figure 10 and many small white vapor bubbles with diameter of about 3–6 $\times$ 10^{-3} m can be observed in the images.

Repeated experiments of pool boiling with distilled water and $CaCO_3$ solution on untreated, polished, and coated surfaces were all carried out and the repeatability was good.

Effect of surface coatings on heat transfer enhancement in pool boiling

Heat transfer enhancement experiments were performed in a pool boiling system with distilled water.

Figure 11 illuminates the relationship between pool boiling heat transfer coefficient of distilled water and running time. It can be found from Figure 11 that, on the one hand, the heat transfer coefficients of various surfaces are basically stable with extension of pool boiling time. On the other hand, heat transfer enhancement can be observed on TiO_2 coating surfaces with thicknesses of 20 $\times$ 10^{-9} m, 60 $\times$ 10^{-9} m, and 80 $\times$ 10^{-9} m compared with those of the untreated surface because heat transfer coefficients on these coated surfaces are higher than those on untreated surfaces, being about 3, 7, and 12% higher, respectively. However, heat transfer deterioration is also obtained on TiO_2 coating surfaces with thicknesses of 40 $\times$ 10^{-9} m and 100 $\times$ 10^{-9} m since on these surfaces heat transfer coefficients are lower than those on untreated surfaces, being about 22 and 19% lower, respectively. The resistance of TiO_2 coatings was estimated on the base of polished surface and is shown in Table 3. Negative value of resistance of TiO_2 coating surface indicates that the boiling heat transfer coefficient of the surface is higher than that of polished surface and pool boiling on such a coated surface is enhanced. The reasons for the experimental phenomena are complex, because there are so many influence factors on the pool boiling process, including the properties of heat transfer surface, distilled water, and heat flux. At specific heat flux and given properties of distilled water, the different properties of heat transfer surface, such as the surface free energy, roughness, topography, etc. contribute to the variation of the heat transfer coefficient. However, no clear explanations can be obtained by analyzing the trends shown in Figures 2, 5, and 6 because they are not in accordance with the tendency of the heat transfer coefficient. Other affecting factors need to be found.

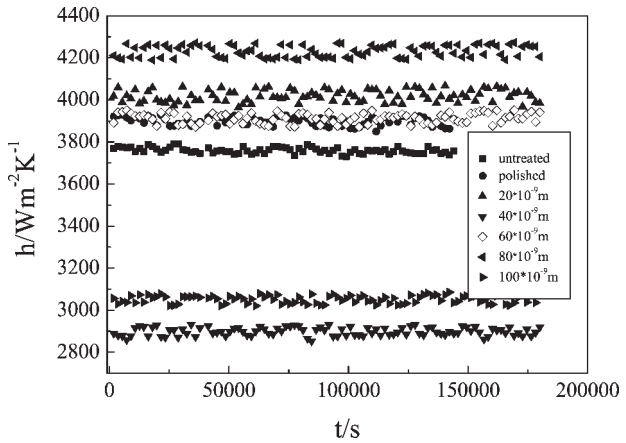

Figure 11. Pool boiling heat transfer coefficient vs. running time for different heat transfer surfaces with distilled water.

It is well known that the more nucleation spots, the more vapor bubbles, and the more violent the pool boiling. The polished surfaces generally provide less nucleation spots than the untreated surfaces, and heat transfer coefficient on polished surface should be lower than that on the untreated surface. Nevertheless, in Figure 11, pool boiling heat transfer coefficient on untreated surface is lower than that on polished surface, which means that polish improves the boiling process in some degree. This experimental result was also obtained in the literature.[19] This may result from the activation effects in micrometer scale on the nucleation spots of the polish process. Similar variation rules are obtained under other heat fluxes.

Table 3. TiO_2 Coating Thickness and Estimated Resistance

$\delta/ \times 10^{-9}$m	$R_f \times 10^6$/W^{-1}m^2 K^1
20	−4.4
40	113
60	6.39
80	−22
100	80.8

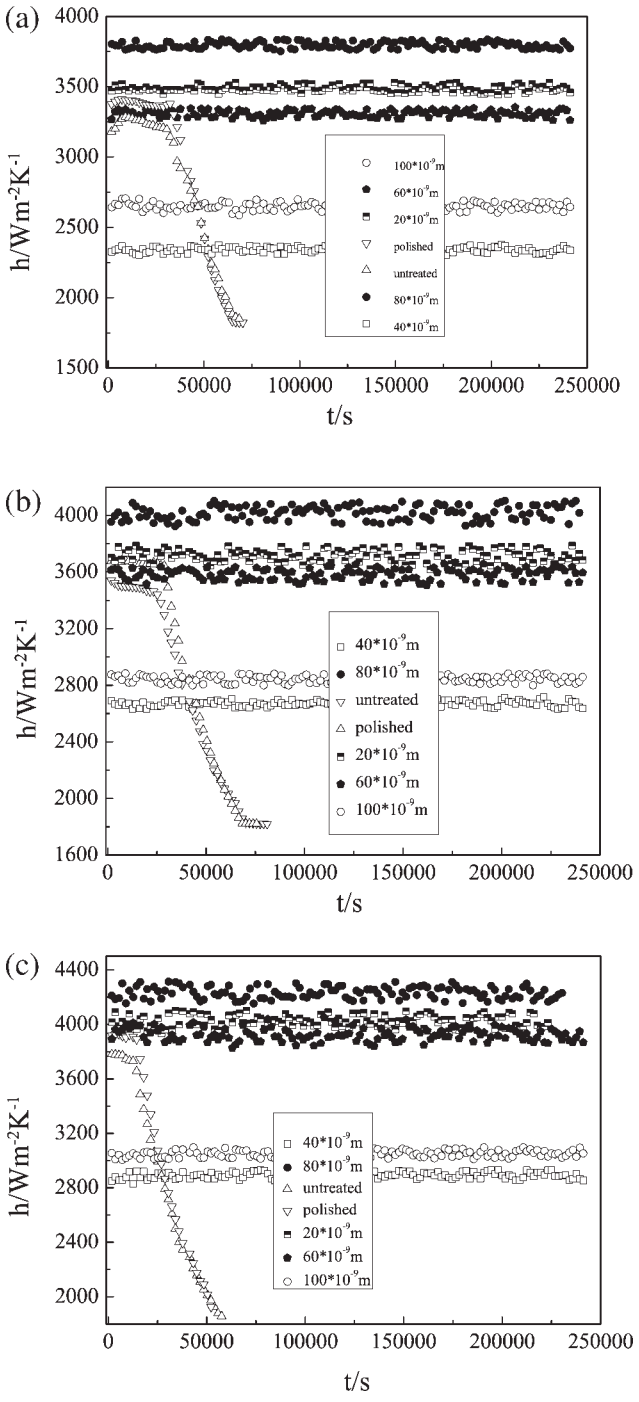

Figure 12. Pool boiling heat transfer coefficients on various heat transfer surfaces vs. running time in $CaCO_3$ water solution.

(a) q = 79.8 kW m^{-2}; (b) q = 96.6 kW m^{-2}; (c) q = 110 kW m^{-2}.

Effect of surface coatings on antifouling in pool boiling

Fouling experiments under pool boiling conditions were performed with $CaCO_3$ water solution.

Figure 12 shows the experimental results of $CaCO_3$ fouling on different heat transfer surfaces, including untreated surface, polished surface, coated surfaces with different TiO_2 coating thickness under various heat fluxes.

It is shown in Figure 12 that in nucleate boiling region, all the TiO_2 coating surfaces have excellent antifouling characteristics compared with untreated and polished surfaces because pool boiling heat transfer coefficient on coated surface basically keeps constant within experimental length of time (about 240,000 s), while those on untreated and polished surfaces drop sharply after only about several hundred minutes and stabilize at low values due to deposits of $CaCO_3$ crystal or fouling on the surfaces. Figure 12 also indicates that surface polish enlarges only slightly fouling induction period, while vacuum coating with TiO_2 in thickness of nanometer scale lengthen fouling induction period greatly. The enhancement effect on antifouling can be contributed in large degree to low surface free energy of nanometer material coatings. Since low-energy surface is less prone to adhesion of crystal and this leads to a lower fouling growth rate on heat transfer surface and a longer induction period. At given operation conditions and solution properties, the different properties of heat transfer surface, such as the surface free energy, roughness, topography, etc. contribute to the variation of the fouling behavior. The roughness value of polished surface is much lower than that of the untreated one. The topography of polished surface is also very different from that of the untreated one. However, it is the surface free energy that plays an important role in the formation of fouling. The two surfaces hold near the same values of surface free energy and it is not surprising that they have almost the same fouling behavior.

In addition, the higher the heat flux, the shorter the fouling induction period for untreated surface or polished surface can be seen in Figures 12a–c, which is easy to be interpreted.

As for the variation rule of pool boiling film coefficient with coating thickness, a tendency that is similar to that of pool boiling of distilled water can be found in Figure 12. That is to say, pool boiling heat transfer coefficient is not a monotonic function of coating thickness variable. As mentioned above, the physical explanation on such tendency is difficult since many factors are responsible for this variation, such as

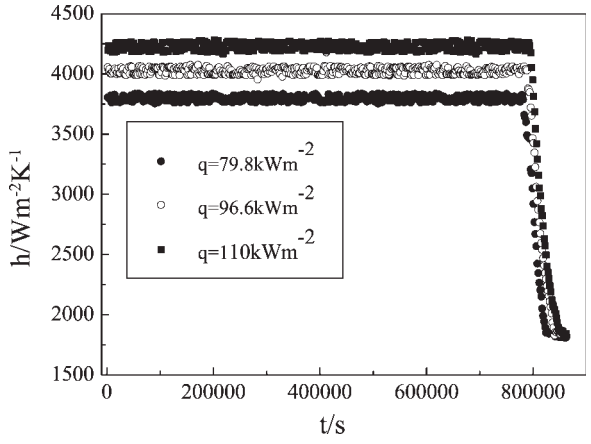

Figure 13. Fouling experiments results on TiO_2 coating surface with layer thickness of 80 × 10^{-9} m in a longer running time.

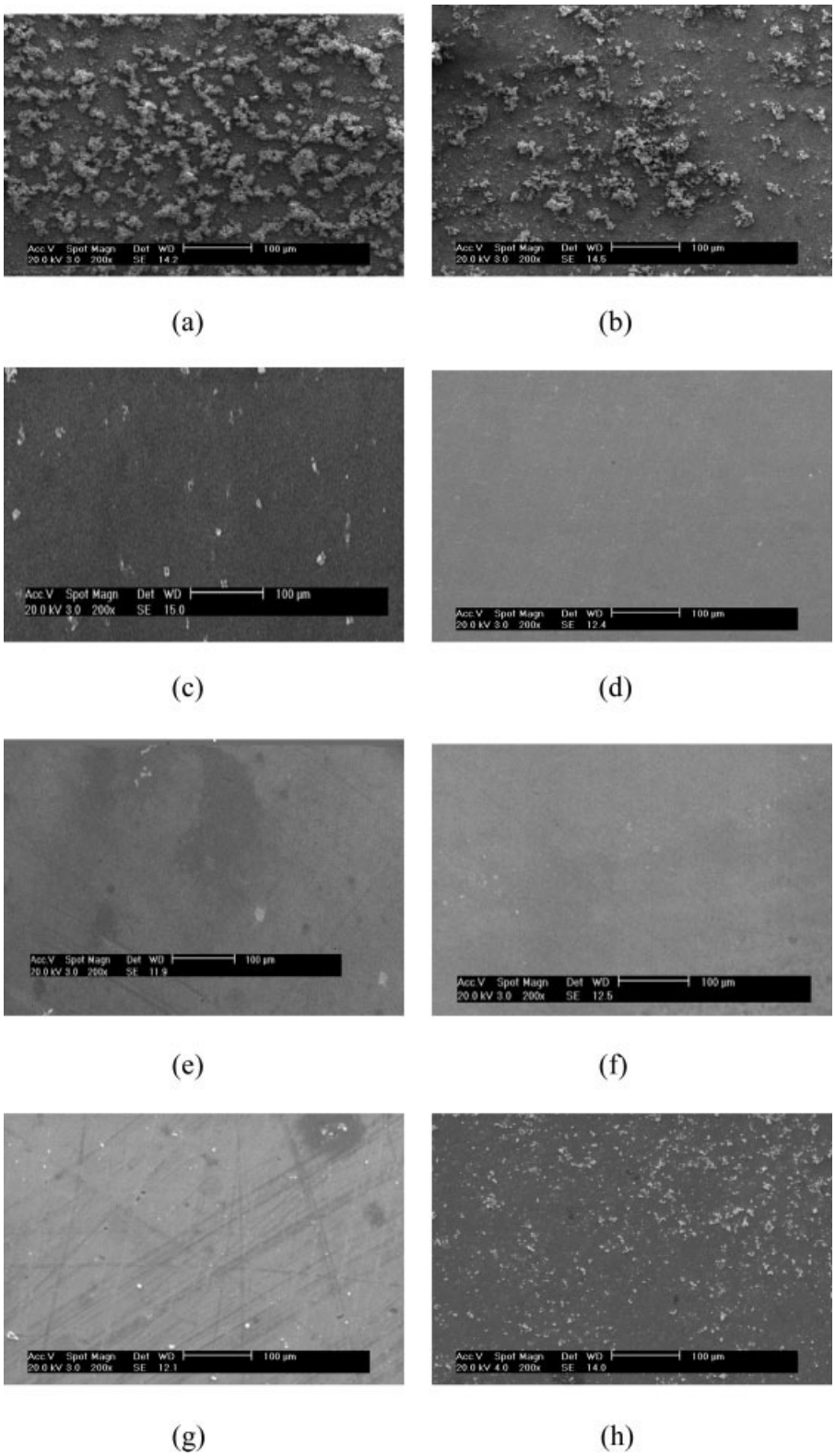

Figure 14. SEM images of $CaCO_3$ scale on untreated, polished and TiO_2 coating surfaces in pool boiling.

(a) Untreated; (b) polished; (c) 100×10^{-9} m; (d) 80×10^{-9} m; (e) 60×10^{-9} m; (f) 40×10^{-9} m; (g) 20×10^{-9} m; (h) 80×10^{-9} m with longer running time.

the surface free energy, topography, roughness, coating method, coating material properties, coating inner nanometer microstructure, nanometer scale effect, etc. The surface free energy is not the only factor that affects the boiling heat transfer and antifouling behavior of TiO_2 coating surface. The surface roughness is generally considered to be one of the most important factors that affect the boiling heat transfer process. However, no clear rule can be drawn from the relationship between the surface roughness (Figure 6) and boiling heat transfer coefficient (Figures 11 and 12). All the coating surfaces have similar topographies. Fouling experiments were repeated and good agreements were found. Some other most possible factors may be the inner nanometer microstructure of TiO_2 coatings, nanometer effect, the condition of vacuum coating process etc. that can lead to different coating thermal resistance or thermal conductivity and different vaporization or boiling mechanism, which needs further identification.

Figures 12a–c indicate that antifouling rules of coated surfaces are similar for different heat fluxes. Besides, under the present experimental conditions, heat transfer coefficient is the largest when the thickness of the coated surface is 80×10^{-9} m and the coated surfaces with certain film thickness (20×10^{-9} m, 60×10^{-9} m, and 80×10^{-9} m) can not only inhibit fouling on heat transfer surface but also enhance the pool boiling heat transfer. However, some coated surfaces (with coating thicknesses of 40×10^{-9} m and 100×10^{-9} m) can only inhibit fouling, which likes most other coatings made of ordinary materials or layer thicknesses.

To investigate the practical durability of the TiO_2 coating surface, the fouling experiments with longer running time were carried out on TiO_2 coating surface with layer thickness of 80×10^{-9} m. The result shows that heat transfer coefficient of pool boiling on 80×10^{-9} m TiO_2 coating surface lasts steadily in a high level about 780,000 s, which is about 50 times longer than that on the untreated surface and after that it drops suddenly to a low level, as shown in Figure 13. The sharp decrease of pool boiling film coefficient may have close relationship with the inherent properties of vacuum coating surface.

After the boiling fouling experiments, the SEM images of untreated, polished, and TiO_2 coating surfaces with different film thicknesses are given in Figure 14, respectively. $CaCO_3$ deposits on these surfaces can be investigated by analyzing Figure 14. Figures 14a, b show that a large amount of $CaCO_3$ scale is formed on untreated and polished surfaces and the deposit of $CaCO_3$ crystal exhibits a packed structure due to the strong adhesion force between scale and heat transfer surface. On the contrary, there is very little deposit on coated surfaces with a loose structure partly due to the weak adhesion force between deposit and coated surface. In the mean while, most TiO_2 coating surfaces were not destroyed and keep their original appearances or surface patterns.

The SEM image of coated surfaces with film thickness of 80×10^{-9} m after a longer running time is also shown in Figure 14h for comparison, and fouling with loose structure on the surface can be found.

Concluding Remarks

Compared with those of the untreated and polished surfaces, surface free energy of the vacuum coating TiO_2 surfaces in nanometer scale thickness drops greatly. However, it reduces slightly when film thickness decreases in nanometer range. Surface free energy depends largely on the inherent property of coating material itself. Compared with that of the untreated surface, the roughness of the TiO_2 coating surfaces including that of the polished surface drops significantly. But, the roughness reduces weakly with the increase of the coating thickness. TiO_2 coating surfaces and polished surface hold the similar morphology, which is very different from that of untreated surface.

All TiO_2 coating surfaces with thickness in nanometer scale can inhibit fouling significantly partly due to their lower surface free energy. Even though it deposits on TiO_2 coating surfaces after a quite long running time, $CaCO_3$ crystal fouling is not serious and exhibits a rather loose structure. The fouling induction period of the TiO_2 coating surface in pool boiling with film thickness of 80×10^{-9} m is about 50 times longer than that of the untreated or polished surface in the present conditions.

Boiling heat transfer enhancement was observed on TiO_2 coating surface with certain coating thickness, such as with film thicknesses of 20×10^{-9} m and 80×10^{-9} m. However, opposite phenomena were also seen.

It seems that besides the surface free energy, roughness, and topography, coating material and method, coating inner nanometer microstructure, nanometer scale effect, interface forces, etc. have significant influence on fouling formation and boiling heat transfer enhancement. Designing finer experimental and measuring system from the point of view of the nanometer scale effect to disclose the process mechanism is further work. In addition, studying the heat transfer enhancing and fouling behaviors of the TiO_2 coating under the exposure of UV is also an interesting subject since the surface contact angle of the TiO_2 coating may be changed from about 0° to 180° when it is exposed or not exposed with UV light and a novel idea or equipment of on-off heat exchanger may be designed.

Acknowledgments

The work is supported by the Cheung Kong Scholar Program for Innovative Teams of the Ministry of Education. (CKSPITME) (No. IRT0641). The authors are grateful to the CKSPITME for the financial support. The authors also thank Profs. Lin Rui-tai and Chen Cai-he and Dr. Du Xi-wen for their kind help in the preparations of the coatings and the pool boiling experiments.

Notation

h = heat transfer coefficient, W m^{-2} K^{-1}
h_0 = heat transfer coefficient on polished heat transfer surface, W m^{-2} K^{-1}
n = point number of temperature measurement
q = heat flux, W m^{-2}
R_f = fouling resistance, W^{-1} m^2 K^1
R_{max} = difference in height between the highest and lowest points on the surface relative to the mean plane, m
R_{rms} = root mean square roughness, m
T = temperature, K
t = time, min

Greek letters

γ = surface free energy, J m^{-2}
δ = thickness of coating layer, m

θ = contact angle,
λ = heat conductivity, $Wm^{-1}\ K^{-1}$
χ = direct distance between measuring points in center axis of heating black, m

Subscripts

g = glycerine as titer
i = certain measuring point
s = saturated
w = distilled water as titer; wall

Literature Cited

1. Branch CA, Muller-Steinhagen H. Influence of scaling on the performance of shell-and-tube heat exchangers. *Heat Transfer Eng*. 1991;12:37–45.
2. Steinhagen R, Muller-Steinhagen H, Maani K. Problems and costs due to heat exchanger fouling in New Zealand industries. *Heat Transfer Eng*. 1993;14:19–30.
3. Hewitt GF, Shires GL, Bott TR. *Process Heat Transfer*. Boca Raton: CRC Press, 1994.
4. Muller-Steinhagen H. Fouling of heat exchanger surfaces. *Chem Ind (London)*. 1995;5:171–174.
5. Aborek J. Assessment of Fouling Research on the Design of Heat Exchanger, Fouling Mitigation of Industrial Heat-Exchanger Equipment. New York: Begell House, 1997.
6. Bott TR, Melo LF, Panchal CB. *Understanding Heat Exchanger Fouling and Its Mitigation*. New York: Begell House, 1999.
7. Muller-Steinhagen H, Malayeri MR, Watkinson A. Fouling of heat exchangers-new approaches to solve an old problem. *Heat Transfer Eng*. 2005;26:1–4.
8. Branch CA, Muller-Steinhagen HM. Study of fouling from Kraft pulp black liquor. *Inst Chem Eng Symp Ser*. 1992;2:1007–1012.
9. Müller-Steinhagen H, Zhao Q. Investigation of low fouling surface alloys made by ion implantation technology. *Chem Eng Sci*. 1997; 52:3321–3332.
10. Bornhorst A, Muller-Steinhagen H, Zhao Q. Reduction of scale formation under pool boiling conditions by ion implantation and magnetron sputtering on heat transfer surfaces. *Heat Transfer Eng*. 1999;20:6–14.
11. Forster M, Bohnet M. Influence of the interfacial free energy crystal/heat transfer surface on the induction period during fouling. *Int J Therm Sci*. 1999;38:944–954.
12. Muller-Steinhagen H, Zhao Q, Helali-Zadeh A, Ren XG. Effect of surface properties on $CaSO_4$ scale formation during convective heat transfer and subcooled flow boiling. *Can J Chem Eng*. 2000;78:12–20.
13. Yang QF, Ding J, Shen ZQ. Scaling and removal of calcium carbonate on electroless plating surface. *Chin J Chem Eng*. 2001;9:150–155.
14. Zhao Q, Liu Y. Investigation of graded Ni-Cu-P-PTFE composite coatings with antiscaling properties. *Appl Surf Sci*. 2004;229:56–62.
15. Zhao Q, Wang X. Heat transfer coated with fluorinated diamond-like carbon films to minimize scale formation. *Surf Coat Technol*. 2005;192:77–80.
16. Santos O, Nylander T, Rosmaninho R, Rizzo G, Yiantsios S, Andritsos N, Karabelas A, Muller-Steinhagen H, Melo L, Boulang L, Boulange-Petermann L, Gabet C, Braem A, Tragardh C, Paulsson M. Modifed stainless steel surfaces targeted to reduce fouling–surface characterization. *J Food Eng*. 2004;64:63–79.
17. Rosmaninho R, Melo LF. Calcium phosphate deposition from simulated milk ultrafiltrate on different stainless steel-based surfaces. *Int Dairy J*. 2006;16:81–87.
18. Gao M, Sun FZ, Shi YT, Lei SH, Niu ZG. Experimental research and theoretical analysis of anti-fouling characteristics on the surface of Ni-based implanted tube. *Int Commun Heat Mass Transfer*. 2006; 33:1115–1121.
19. Ren XG, Li TF, Zhao Q, Muller-Steinhagen H. Investigation of $CaSO_4$ scale formation under pool boiling. *Chem Eng (China)*. 2006;34:13–16.
20. Rosmaninho R, Santos O, Nylander T, Paulsson M, Beuf M, Benezech T, Yiantsios S, Andritsos N, Karabelas A, Rizzo G, Muller-Steinhagen H, Melo L. Modified stainless steel surfaces targeted to reduce fouling-Evaluation of fouling by milk components. *J Food Eng*. 2007;80:1176–1187.
21. Bergles AE. Enhancement of pool boiling. *Int J Refrigeratio*. 1997; 20:545–551.
22. Scurlock RG. Enhanced boiling heat transfer surfaces. *Cryogenics*. 1995;35:233–237.
23. Hsieh SS, Weng CJ. Nucleate pool boiling from coated surfaces in saturated R-134a and R-407c. *Int J Heat Mass Transfer*. 1997;40: 519–532.
24. Webb RL, Donald Q. Kern lecture award paper: odyssey of the enhanced boiling surface. Transactions of the ASME. *J Heat Transfer*. 2004;126:1051–1059.
25. Gorenflo D, Kotthoff S, Danger E, Luke A. Heat transfer and bubble formation in pool boiling: effect of basic surface modifications for heat transfer enhancement. *Int J Therm Sci*. 2006;45:217–236.
26. Liu AL, Xu H, Wang XS, Zhou JX, Hou F, Wang C. Boiling heat transfer on composite powder porous surface tubes. *J Chem Ind Eng (China)*. 2006;57:726–730.
27. Vemuri S, Kim KJ. Pool boiling of saturated FC-72 on nano-porous surface. *Int Commun Heat Mass Transfer*. 2005;32:27–31.
28. Takata Y, Hidaka S, Cao JM, Tanaka K, Masuda M, Ito T, Watanabe I, Shimohigoshi M. Boiling and evaporation from a superhydrophilic surface. *Therm Sci Eng*. 2000;8:33–41.
29. Takata Y, Hidaka S, Masuda M, Ito T. Pool boiling on a superhydrophilic surface. *Int J Energy Res*. 2003;27:111–119.
30. Takata Y, Hidaka S, Cao JM. Effect of surface wettability on boiling and evaporation. *Energy*. 2005;30:209–220.
31. Takata Y, Hidaka S, Uraguchi T. Boiling feature on a super water-repellent surface. *Heat Transfer Eng*. 2006;27:25–30.
32. Gao XF, Jiang L. Recent studies of natural superhydophobic biosurfaces. *Physics*. 2006;35:559–564.
33. Liu MY, Wang H, Wang Y. Enhancing flow boiling and antifouling with nanometer titanium dioxide coating surfaces. *AIChE J*. 2007; 53:1075–1085.
34. Michalski MC, Hardy J, Saramago BJ. On the surface energy of PVC/EVA polymer blends comparison of fifferent calculation methods. *J Colloid Interface Sci*. 1998;208:319–328.
35. Bang IB, Chang SH. Boiling heat transfer performance and phenomena of Al_2O_3-water nano-fluids from a plain surface in a pool. *Int J Heat Mass Transfer*. 2005;48:2407–2419.

Manuscript received May 4, 2007, and revision received Sept. 21, 2007.